Transfer-matrix algorithm for the calculation of the band structure of semiconductor superlattices

L. R. Ram-Mohan
Department of Physics, Worcester Polytechnic Institute, Worcester, Massachusetts 01609

K. H. Yoo and R. L. Aggarwal*
Francis Bitter National Magnet Laboratory and Department of Physics, Massachusetts Institute of Technology, Cambridge, Massachusetts 02139
(Received 21 March 1988; revised manuscript received 18 July 1988)

A new compact algorithm has been developed for the calculation of the band structure of III-V or II-VI compound semiconductor superlattices. Within the envelope-function approximation, the procedure yields a transfer matrix of dimension $2n \times 2n$ for an n-band $\mathbf{k}\cdot\mathbf{p}$ model. The boundary conditions for the wave functions at the interfaces between layers are built into the calculation in a natural manner. The method readily adapts itself to the case where an external magnetic field is present along the superlattice axis. The effects of strain, due to lattice mismatch or an applied external stress, can also be taken into account. This extended transfer-matrix method enjoys the advantages of the usual one-band transfer-matrix method which is employed in solving the Kronig-Penney model. The standard eight-band $\mathbf{k}\cdot\mathbf{p}$ description of the band structures of the individual layers is used in obtaining results for specific superlattices. Our results are in excellent agreement with earlier calculations which have used the $\mathbf{k}\cdot\mathbf{p}$ and the tight-binding approximations.

I. INTRODUCTION

Semiconductor superlattices and submicrometer heterostructures are of interest not only for their device applications but also for the fundamental physical phenomena they exhibit due to their material properties and their submicrometer dimensions. In order to understand the features exhibited in the optical and magnetooptical spectra of superlattices, it is essential to calculate their electronic band structure. Two methods have been commonly used for such calculations. One is the tight-binding approximation,[1-8] which is able to include the contributions from the entire Brillouin zone of the bulk materials in calculating the zone-folded bands in superlattices. The second method for the band structure is the envelope-function approximation (EFA),[9-15] which is an adaptation of the $\mathbf{k}\cdot\mathbf{p}$ approximation[16] used in the theory of band structure of bulk semiconductors. The EFA is essentially the effective-mass approximation in the context of superlattices. This approximation has the advantage of being adaptable to the case where an external magnetic field is imposed.

The problem of solving for the band structure within EFA reduces to the solution of a set of simultaneous second-order differential equations for the envelope functions. The number of simultaneous equations depends on the number of energy bands of the bulk material which is taken into consideration. In this paper we present the theory for a compact numerical algorithm for the evaluation of the band structure and wave functions for semiconductor superlattices within a multiple-band EFA.

The EFA is elaborated on in Sec. II. We present our algorithm and show how the boundary conditions[9,10] are built into the procedure in a natural manner. The procedure implemented for the multiple-band situation has the advantages associated with the usual transfer-matrix approach, which has been used so extensively in the context of the one-dimensional Kronig-Penney model.[17] Thus our extension of the transfer-matrix method permits the calculation of the energy spectrum and the wave functions for superlattices of arbitrary dimensions and layer interleaving. Essential features of the earlier work by Bastard[9,10] and by Altarelli[12-14] are discussed, and contrasted with the present computational procedure. The advantage of the proposed transfer-matrix approach is its conceptual simplicity together with compactness as an algorithm. At the same time it retains the usual advantages, associated with the EFA, of incorporating (a) the effect of an applied magnetic field, and (b) the effect of strain, which may be present in superlattice layers due to lattice mismatch across interfaces or due to applied stress. Results from sample calculations are discussed in Sec. III for GaAs/$Ga_{1-x}Al_xAs$ and HgTe/CdTe superlattices and are compared with those published previously using a variational procedure[14] within the EFA and the tight-binding approximation.[8]

II. THE TRANSFER-MATRIX METHOD

A. The envelope functions for superlattices

Let us consider the case of a semiconductor superlattice made up of alternating planar layers of materials A and B of thicknesses d_1 and d_2, respectively. Both A and B are taken to be from either the III-V compound semiconductors, such as GaAs and $Ga_{1-x}Al_xAs$, or the II-VI compound semiconductors, such as HgTe and $Hg_{1-x}Cd_xTe$. In these materials the conduction- and

valence-band edges relevant to optical and transport properties have Γ_6, Γ_7, or Γ_8 symmetry. The periodic parts of the Bloch functions $u_{j,\mathbf{k}=0}(\mathbf{r})$ at the band edges, where j is the band index, do not differ very much as we go from layer to layer. Also, the original crystal symmetry is maintained in the planes parallel to the the layers. Let the z axis of the Cartesian coordinate system be perpendicular to the layers, with the x-y plane being parallel with the layers.

We shall assume that the band structures of the bulk materials are well described by a $\mathbf{k}\cdot\mathbf{p}$ Hamiltonian at the center of the Brillouin zone. We include the $J=\frac{3}{2}$ heavy-hole (hh) and light-hole (lh) bands, and the $J=\frac{1}{2}$ spin-orbit split-off (s.o.) valence bands together with the Γ_6 conduction bands, in an eight-band description of the band structure of bulk materials. Within the context of this eight-band Kane model we assume that the wave functions $\Psi^{(A,B)}_{(\nu,\mathbf{k})}(\mathbf{r})$ in each layer satisfying the relation

$$H^{(A,B)}\Psi^{(A,B)}_{(\nu,\mathbf{k})}(\mathbf{r})=\varepsilon^{(A,B)}_{\nu,\mathbf{k}}\Psi^{(A,B)}_{(\nu,\mathbf{k})}(\mathbf{r}) , \tag{1}$$

can be written in the form

$$\Psi^{(A,B)}_{(\nu,\mathbf{k})}(\mathbf{r})=\sum_j F^{(A,B)}_{\nu,\mathbf{k},j}(\mathbf{r})u_{j,\mathbf{k}=0}(\mathbf{r}) , \tag{2}$$

where we have assumed that $u^A=u^B$. In the EFA, which is analogous to the effective-mass approximation in bulk materials, we consider the envelope functions $F^{(A,B)}_j(\mathbf{r})$ to be slowly varying over the unit cells of the lattice. For convenience we have omitted the subscripts $\nu,\mathbf{k}$ on $F(\mathbf{r})$.

In the superlattice we have the additional potentials $V_S(z)$ and $V_P(z)$, with period $d=d_1+d_2$, which arise from the band offsets for the conduction- and valence-band edges across an interface due to the mismatch of the band gaps as one goes across the interface.

In order to understand the implications of the EFA it is instructive to follow the calculation of Luttinger and Kohn,[18] who obtained the effective-mass approximation for the impurity potential in bulk semiconductors, and to repeat it for the potentials $V_{S,P}(z)$ for the superlattice. We assume that $V_{S,P}(z)$ are constants in each layer, so that the smoothness of the potentials needed for the validity of the effective-mass approximation is guaranteed. The boundary conditions at the interfaces then ensure that the wave function and the particle probability current are continuous. We might mention that the Luttinger-Kohn treatment of the impurity problem provides a procedure for systematically accounting for corrections to the effective-mass approximation; the same procedure may be employed in the context of superlattices in order to go beyond the EFA.

With the original symmetry surviving in the x and y directions we use the form

$$F_j(\mathbf{r})=e^{ik_x x}e^{ik_y y}f_j(z) \tag{3}$$

for the envelope functions. In the following, we shall work in this representation and the envelope function will refer to the functions $f_j(z)$. In the presence of a magnetic field along the z direction, the in-plane component of the envelope function $e^{ik_x x}e^{ik_y y}$ is replaced by a harmonic oscillator wave function to account for the Landau quantization as will be discussed in Sec. III.

The differential equation satisfied by the envelope functions in each layer is then given by

$$\sum_{j'}[H^{(A,B)}_{jj'}(k_x,k_y,-i\partial/\partial z)+V^{(A,B)}_{jj'}(z)]\times f^{(A,B)}_{j'}(z)=\varepsilon^{(A,B)}f^{(A,B)}_j(z) , \tag{4}$$

where $V^{(A,B)}$ is a matrix with diagonal matrix elements $V_S(z)$ for the conduction-band components and $V_P(z)$ for the valence-band components of f_j. The variables k_x and k_y in the Hamiltonian H are the usual wave-vector eigenvalues, and the k_z dependence has been written as a derivative in the coordinate representation. The matrix elements of $H^{A,B}$ are expressed in terms of the band-edge energies E_g and Δ relative to the valence-band edge, the interband momentum matrix element p, the conduction-band Kane parameter F, and the Luttinger-type[19,20] valence-band parameters γ_1, γ_2, γ_3, and κ. The Luttinger parameter q is found to be negligibly small and therefore is neglected in our calculations. In addition, we have neglected all inversion asymmetry parameters in the Hamiltonian, associated with lack of inversion symmetry in III-V and II-VI compounds. The neglect of these small terms leads to a Kramers degeneracy for the bands, which is not lifted in a superlattice even for $k_x\neq 0$. In principle, this can be rectified by including these terms in our Hamiltonian. We employ the phase conventions and notation defined by Weiler[21] for the Bloch functions $u_{j,\mathbf{k}=0}(\mathbf{r})$. Thus the matrix elements of the Hamiltonian H are identical with the ones given in Table II of Ref. 21. We reproduce the matrix elements of H, with only the parameters relevant to our work, in the Appendix.

Equation (4) is a set of eight coupled second-order differential equations in the variable z. We reexpress it as

$$\left[-\mathcal{A}_{jj'}\frac{\partial^2}{\partial z^2}-i\mathcal{B}_{jj'}\frac{\partial}{\partial z}+\mathcal{C}_{jj'}\right]f_{j'}(z)=\varepsilon f_j(z) , \tag{5}$$

where $\mathcal{A}$, $\mathcal{B}$, and $\mathcal{C}$ are matrices with coefficients obtained from Eq. (4).

The first boundary condition on f_j is that they be continuous across any interface. By integrating Eq. (5) from one side of an interface to the other, assuming that the discontinuities of the potential functions are finite, we obtain the condition[9,10] that $-\mathcal{A}f'-i\mathcal{B}f$ has to be continuous across any interface.

It is convenient to rewrite Eq. (5) as a set of 16 simultaneous first-order differential equations for the 16-component function $\Phi(z)$ defined by

$$\Phi(z)=\begin{bmatrix} f_j(z) \\ -\mathcal{A}f'_j(z)-i\mathcal{B}f_j(z)\end{bmatrix} . \tag{6}$$

The continuity conditions on f and their derivatives are assured by requiring that $\Phi(z)$ be continuous across any interface. This is easily done since Φ satisfies a first-order differential equation in each layer and we set $\Phi(z-0^+)=\Phi(z+0^+)$ at any interface. Equation (5) can be rewritten as

$$\Phi'(z)=\begin{bmatrix} -i\mathcal{A}^{-1}\mathcal{B} & -\mathcal{A}^{-1} \\ \varepsilon-\mathcal{C} & 0 \end{bmatrix}\Phi(z)\equiv\Lambda\Phi(z) \ . \tag{7}$$

A unique solution to Eq. (7) is given by

$$\Phi(z)=\exp(\Lambda z)\Phi(0)=\mathcal{T}(z)\Phi(0) \ . \tag{8}$$

Here $\Phi(z)$ is obtained, in terms of an initial value at $z=0$, by the 16×16 "transfer matrix" $\mathcal{T}(z)$. We discuss the details of the evaluation of the exponential matrix $\mathcal{T}$ below. It depends on the band parameters in the layer over which it is evaluated, and on the energy eigenvalue ε.

The Bloch periodicity of the envelope functions and their derivatives over the period (d_1+d_2) requires that the function Φ satisfy the condition

$$\Phi(d_1+d_2)=\exp[iq(d_1+d_2)]\Phi(0) \ , \tag{9}$$

where q is the superlattice wave vector parallel to the z axis. On the other hand, the use of transfer matrices leads to the expression

$$\Phi(d_1+d_2)=\mathcal{T}(d_2)\mathcal{T}(d_1)\Phi(0)=\mathcal{T}_{\rm tot}(d_1,d_2)\Phi(0) \ . \tag{10}$$

Comparing Eqs. (9) and (10) we obtain an eigenvalue equation

$$\mathcal{T}_{\rm tot}(d_1,d_2)\Phi(0)=\exp(iqd)\Phi(0) \ . \tag{11}$$

This condition is satisfied with real q only for physically allowed values of ε. The allowed values of ε are obtained by scanning in energy and performing a diagonalization of the total transfer matrix on the left-hand side of Eq. (11) to see if any eigenvalue equals $\exp(iqd)$ for a given fixed value of q. This allows us to solve for the ε versus q relation for all the superlattice bands.

B. Numerical procedure

The evaluation of $\exp(\Lambda z)$, of Eq. (8), is central to the transfer-matrix method. Let the diagonalized form of Λ be labeled by λ. Let the matrix $\mathcal{P}$ be the transformation matrix which diagonalizes Λ such that

$$\mathcal{P}^{-1}\Lambda\mathcal{P}=\lambda \ . \tag{12}$$

We can then construct the exponential matrix using the relation

$$\mathcal{T}(z)=\exp(\Lambda z)=\mathcal{P}\exp(\lambda z)\mathcal{P}^{-1} \ . \tag{13}$$

Within the $\mathbf{k}\cdot\mathbf{p}$ approximation the presence of large values for λ_j in Eq. (13) is inappropriate and has to be modified. They can lead to numerical overflow on exponentiation or to spurious superlattice bands even though they do not contribute to a real superlattice band. We introduce a cutoff wave vector λ_c so that if $|\lambda_j|\geq\lambda_c$, then λ_j is replaced by $(\mathrm{sgn}\lambda_j)\lambda_c$. Real and spurious bands can be distinguished easily since a real band remains the same when we change λ_c whereas a spurious band is very sensitive to λ_c. Typically, we use $0.1-0.3$ Å^{-1} for λ_c.

The typical matrix under consideration is of dimension 16, so that the computer memory requirements are modest for this calculation. We employ standard subroutines available in the EISPACK and LINPACK mathematical subroutine libraries,[22,23] in order to first diagonalize Λ and obtain the matrix $\mathcal{P}$ of eigenfunctions of Λ, and then to calculate the inverse of $\mathcal{P}$. It is well known that considerable care is necessary in order to obtain the exponential of an arbitrary matrix.[24] We account for possible degeneracies in λ by employing a Gram-Schmidt orthogonalization procedure while constructing $\mathcal{P}$. The accuracy of the matrix diagonalization and of the matrix inversion procedures are monitored through a convergence criterion for the eigenvalues and through a parameter for determining the condition of the matrix. With the use of extended numerical precision in the analysis, we conservatively estimate the accuracy of the final energy eigenvalues to be about 1 part in 10^8.

The wave function is obtained, for a physically acceptable energy value, by diagonalizing a total transfer matrix [see Eq. (11)]. The initial value at $z=0$ of the wave function is the eigenfunction corresponding to that eigenvalue which equals $\exp(iqd)$. The wave functions at specified values of z in the region of interest are given by constructing the corresponding transfer matrices which will transform the wave function at the initial value to the one at z.

A comparison of the transfer-matrix method with numerical procedures employed earlier is in order. Bastard[9,10] has reduced the eight simultaneous differential equations (5) for f_j into a single differential equation for a given band by eliminating other component functions by repeated substitution. For a successful elimination of other components the $\mathbf{k}\cdot\mathbf{p}$ Hamiltonian is restricted to first-order terms in k. This elimination may be viewed as a procedure which employs a "condensation" of equations to just one equation. This single equation is then solved as a standard Kronig-Penney[17] problem. It should be noted that the original method used by Bastard[9,10] is mathematically inconsistent because terms of second-order in k are neglected in the $\mathbf{k}\cdot\mathbf{p}$ Hamiltonian but are retained after applying the condensation method. The usual boundary conditions on the continuity of f_j and its derivative are then applied to this new second-order differential equation. This approximation is numerically inaccurate, giving band gaps which deviate from the correct values; for example, for a HgTe/CdTe superlattice of layer thicknesses (61 Å)/(25 Å) with an assumed valence-band offset of 40 meV, the Bastard model yields a band gap in excess of 86 meV which may be compared with a more precise value of 51 meV obtained from the transfer-matrix method. An additional limitation inherent in the Bastard approach of condensation of equations is that it is incapable of including the spin splitting of levels due to an external magnetic field. Thus the Bastard approach will provide inaccurate results for superlattices made up of narrow gap materials with electrons and holes having large g factors. On the other hand, in our method the inclusion of the spin splitting terms does not alter the basic structure of the simultaneous second-order differential equations [Eq. (5)]. The only change needed is that the matrices $\mathcal{B}$ and $\mathcal{C}$ are now rewritten in terms of the creation and annihilation operators of the Landau harmonic oscillator states; thus the transfer-

matrix carries over intact even with magnetic field being present.

Altarelli[12–14] uses a variational procedure by defining an action integral having a $2j\times 2j$ Hamiltonian in which the $\mathbf{k}\cdot\mathbf{p}$ Hamiltonians of the two layers A and B are entered in block-diagonal form. The boundary conditions are included by having an additional term called the "interface functional" in the action integral. The solutions for the energy bands and wave functions are then obtained by requiring that the action integral be an extremum under small variations in $f_j^{(A,B)}$. The numerical procedure requires (a) the calculation of $(2\times j\times m)^2$ matrix elements, where j is the number of bands and m is the number of interpolation functions used to represent the $f_j^{(A,B)}$, (b) the diagonalization of a matrix of dimension $2\times j\times m$, and (c) an iterative procedure involving diagonalization in order to arrive at the minimum in energy with acceptable accuracy. A typical number of interpolation functions used is 6–10, leading to matrices of dimensions 72–120, so that this algorithm requires larger computer memory than our method.

III. APPLICATIONS

In this section, we compare the results of our calculations with the transfer-matrix method for $GaAs/Ga_{1-x}Al_xAs$ and HgTe/CdTe superlattices with those of Altarelli[14] for $GaAs/Ga_{1-x}Al_xAs$ and those of Schulman and Chang[8] for HgTe/CdTe.

A. The $GaAs/Ga_{1-x}Al_xAs$ superlattice at zero magnetic field

The band parameters used in our numerical work are determined as follows. The energy gap for $Ga_{1-x}Al_xAs$ is calculated from the band gap for GaAs using the relation[25]

$$E_g(x)=E_g(0)+1.04x+0.47x^2 \quad \text{for } x<0.4 . \tag{14}$$

The other parameters for $Ga_{1-x}Al_xAs$ for a given x are obtained by a linear interpolation of the values[26] for GaAs ($x=0$) and AlAs ($x=1$) shown in Table I. The currently accepted value[27] of the conduction-band offset, V_s, for $GaAs/Ga_{1-x}Al_xAs$ heterostructures is 60% of the difference ΔE_g in band gaps in two adjacent layers. However, in order to compare numerical results with the earlier work of Altarelli[14] we have deliberately worked with V_s having a value[28] of 85% of ΔE_g. We explicitly include the s.o. band in our calculation, while in Ref. 14 it is accounted for only indirectly by using a modified conduction-band mass.[29]

TABLE I. The band parameters of GaAs and AlAs (after Ref. 26).

	GaAs	AlAs
E_g (eV)	1.521	
E_P (eV)	25.7	21.1
Δ (eV)	0.34	0.275
γ_1^L	6.85	3.45
γ_2^L	2.10	0.68
γ_3^L	2.90	1.29
κ^L	1.20	0.12

We have calculated the band structure for a $GaAs/Ga_{0.79}Al_{0.21}As$ superlattice with layer thicknesses of (125 Å)/(80 Å) using our transfer-matrix method. In Fig. 1 we show the band structure (dashed lines) obtained with the spherical approximation in order to facilitate comparison with the results of Altarelli.[14] The spherical approximation, which neglects the warping of the bulk valence bands, replaces γ_2 and γ_3 by the value

$$\bar{\gamma}=\frac{2\gamma_2+3\gamma_3}{5} . \tag{15}$$

The results shown in Fig. 1 are in overall agreement with those of Altarelli. There are several small differences. In Ref. 14, (i) the valence subbands hh1, lh1, and hh2 show higher dispersion, (ii) the band-edge energies vary by small amounts from our values, and (iii) the light-hole band labeled ll1 has a maximum away from $k_x=0$, but this feature is more pronounced in Ref. 14. This can be understood in terms of the proximity of ll1 to hh2—the repulsion is larger when the bands are closer as in Ref. 14.

For completeness, we present in Fig. 1 the band structure (solid lines) for the same superlattice without the spherical approximation. The valence subband energies are appreciably different. This is because the band-edge

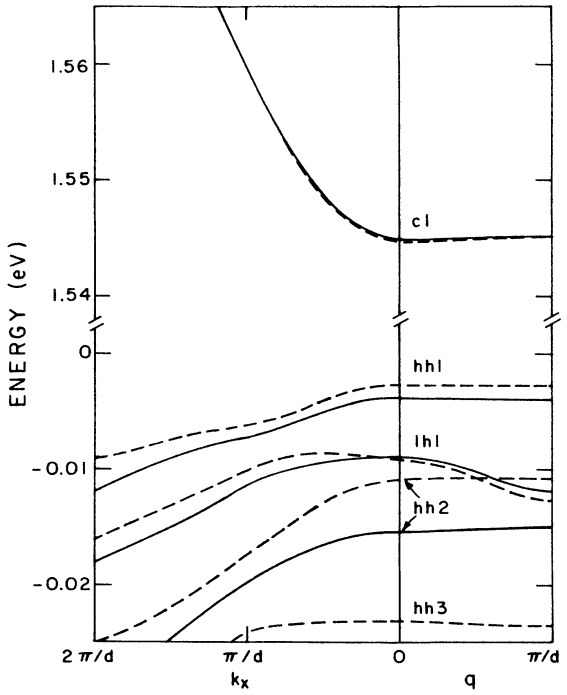

FIG. 1. The band structure of a $GaAs/Ga_{0.79}Al_{0.21}As$ superlattice with growth axis along [001] and layer thicknesses (125 Å)/(80 Å). Band dispersion in the [001] (q) and [100] (k_x) directions is shown with the spherical approximation (dashed lines), and without the spherical approximation (solid lines).

values are sensitive to the input values of γ_1 and γ_2, with the higher subband edges being more so.[13] This fact can be verified easily at least for the hh band since, at $q=0$, it is determined by a Kronig-Penney-type equation with $m_{\parallel}^{*}=1/(\gamma_1-2\gamma_2)$. The k_x dependence is less pronounced here, with the band edges for the light and heavy holes being further apart. Also, the band crossing between the hh2 and lh1 bands along the q direction, present in the spherical approximation, does not manifest itself here.

B. The Landau-level structure in a GaAs/$Ga_{1-x}Al_xAs$ superlattice

We now use the transfer-matrix method to evaluate the effects of an external magnetic field **B**, parallel to the superlattice growth axis. This problem has been discussed at length by Altarelli and co-workers.[12–14] In the $\mathbf{k}\cdot\mathbf{p}$ approximation $\hbar\mathbf{k}$ is replaced by the minimal gauge substitution $[\hbar\mathbf{k}+(e/c)\mathbf{A}]$, and the electron's spin energy in the external field is included explicitly in the Hamiltonian. Here **A** is the vector potential of the applied magnetic field, $\hbar$ is Planck's constant, e is the electronic charge, and c is the velocity of light. The wave-vector components k_x and k_y are now expressed in terms of harmonic oscillator creation and annihilation operators

$$k_x=\left[\frac{eB}{2\hbar c}\right]^{1/2}(a+a^{\dagger}) , \tag{16}$$

$$k_y=i\left[\frac{eB}{2\hbar c}\right]^{1/2}(a-a^{\dagger}) . \tag{17}$$

As before, the component k_z which is along the direction of the applied magnetic field is replaced by $-i\partial/\partial z$. The envelope functions F_j are now products of harmonic oscillator wave functions ϕ_n multiplied by the envelope functions f_j. The complete eight-component wave function for a given Landau level n with a band index ν is written as

$$\Psi(\nu,q,n)=(f_{\nu,1}(z)\phi_n u_1,\ f_{\nu,2}(z)\phi_{n-1}u_2,\ f_{\nu,3}(z)\phi_{n+1}u_3,\ f_{\nu,4}(z)\phi_{n+1}u_4 ,$$
$$f_{\nu,5}(z)\phi_{n+1}u_5,\ f_{\nu,6}(z)\phi_n u_6,\ f_{\nu,7}(z)\phi_{n+2}u_7,\ f_{\nu,8}(z)\phi_n u_8) . \tag{18}$$

Here the index n runs over the values $n=-2, -1, 0, 1, \ldots$, and the component functions f_j are automatically zero for those components which have harmonic oscillator function ϕ_n with n negative.

The entire 8×8 Hamiltonian of Eq. (4) can be written in terms of the creation and annihilation operators and the matrix elements reexpressed in terms of harmonic oscillator matrix elements.[20,21,30] In the Pidgeon-Brown analysis it was natural to decouple the 8×8 Hamiltonian into two block diagonal 4×4 matrices for $k_z=0$. This simplification is no longer applicable since the energy levels in the superlattice, even at $q=0$, obtain contributions from $k_z\neq0$ regions of the bulk material Brillouin zones of the individual layers.

The differential equations satisfied by f_j are again of second order. The transfer-matrix method is again applicable and we calculate the magnetic field dependence of the Landau levels for $q=0$. The results of our calculations for a GaAs/$Ga_{0.79}Al_{0.21}As$ superlattice, with layer thicknesses of (125 Å)/(80Å), are shown in Fig. 2, which may be compared with Fig. 6 of Ref. 14. We have not used the spherical approximation and we have included the s.o. valence bands in the analysis, as before.

The general agreement between the two computational schemes is good. The differences in the valence-band levels are attributable mainly to the use of the spherical approximation and also to the indirect inclusion of the s.o. band in Ref. 14.

C. The HgTe/CdTe superlattice

Here we wish to compare the band structures obtained from the transfer-matrix method in the EFA with those

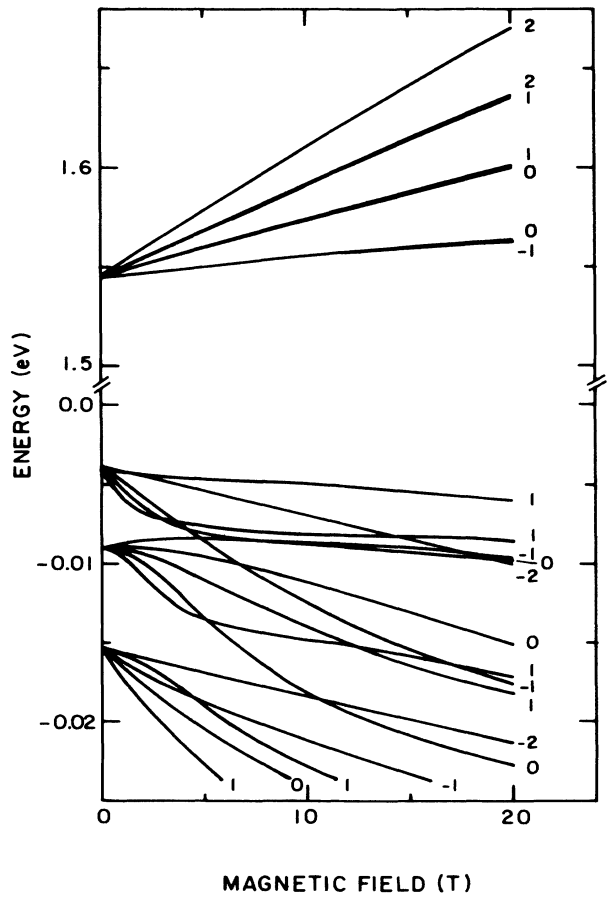

FIG. 2. The Landau-level diagram at $q=0$ for the same superlattice as in Fig. 1.

obtained from the tight-binding model calculations[8] for the HgTe/CdTe superlattices. In order to make this comparison we have assumed that the valence-band offset between HgTe and CdTe is 40 meV. Recent experimental[31] and theoretical[32] indications are that this offset is closer to 350 meV. The other band parameters[21] for HgTe and CdTe are given in Table II.

In Fig. 3(a) we present the band structure of a (50 Å)/(40 Å) HgTe/CdTe superlattice grown along the [001] direction. This may be compared with Fig. 3(a) of Ref. 8. The agreement at the band threshold values at $q=0$ and at the Brillouin-zone boundary along the [001] direction is within 3 meV. The main feature we do not reproduce is the anticrossing of the bands labeled lh1 and hh2 in the q direction. This is due to the absence of small inversion asymmetry terms in our Hamiltonian. In the k_x direction, the hh1 band displays the same behavior in both results. However, the lh1 and the hh2 bands are pulled down lower in our calculation and at $k_x=0.08(\pi/a)$ the two bands in our Fig. 3(a) are about 19 meV lower. Again, not having included inversion asymmetry effects in our calculations, the bands are doubly degenerate due to Kramers's degeneracy even for $k_x\neq 0$.

The effect of strain, due to lattice mismatch between HgTe and CdTe layers with lattice constants 6.462 and 6.482 Å, respectively, can be readily incorporated into our band-structure calculations. This requires a knowledge of the dilatation deformation-potential constants C and a for the conduction- and valence-band edges, respectively, and the shear deformation-potential constants b and d for the valence-band edge of HgTe for the superlattice grown on CdTe substrates. Yoshizaki and Tanaka[33] have measured $b=-1.5$ eV and $d=-2.1$ eV, and Takita and Landwehr[34] have measured $a=+3.8$ eV for HgTe, using the sign convention of Bir and Pikus.[35] According to this value of a, the energy of the valence-band edge of HgTe should *increase* with pressure. However, on the basis of the tight-binding model, Wu[36] argues that the energy of the valence-band edge of HgTe should *decrease* with pressure. On the other hand, the temperature coefficient of the energy gap in HgTe has been measured[26] to be $dE_g/dT=+5\times10^{-4}$ eV/K. If dE_g/dT was entirely due to the change in the lattice parameter with temperature, then dE_g/dT should be negative on the basis of the tight-binding model. Thus it is not clear whether the arguments for the spin of a based on the tight-binding model are entirely appropriate. The value for the conduction-band deformation potential C can be deduced from the relationship

$$C=-a-\tfrac{1}{13}(c_{11}+c_{12})\frac{dE_g}{dp}\ , \tag{19}$$

where $c_{11}=5.92$ N/m^2 and $c_{12}=4.14$ N/m^2, as measured by Apler and Saunders,[37] and dE_g/dp is the pressure coefficient of the band gap. Taking $\frac{1}{2}(c_{11}+c_{12})=4.74\times10^5$ bars, and $dE_g/dp=12\times10^{-6}$ eV/bar as in Ref. 38, we obtain $C=-9.49$ eV. Figure 3(b) shows the result of including strain for the same superlattice as in Fig. 3(a). It should be noted that the entire spectrum in Fig. 3(b) has been shifted down by -8

TABLE II. The band parameters of HgTe and CdTe used in our calculation (from Ref. 21). The valence-band parameters shown here have already been adjusted for the explicit inclusion of the conduction-band contributions to the valence-band effective masses.

	HgTe	CdTe
E_g (eV)	−0.304	1.608
E_P (eV)	19.0	19.0
Δ (eV)	1.0	1.0
F	−0.8	−0.8
γ_1	3.3	3.3
γ_2	0.1	0.1
γ_3	0.9	0.9
κ	−0.8	−0.8

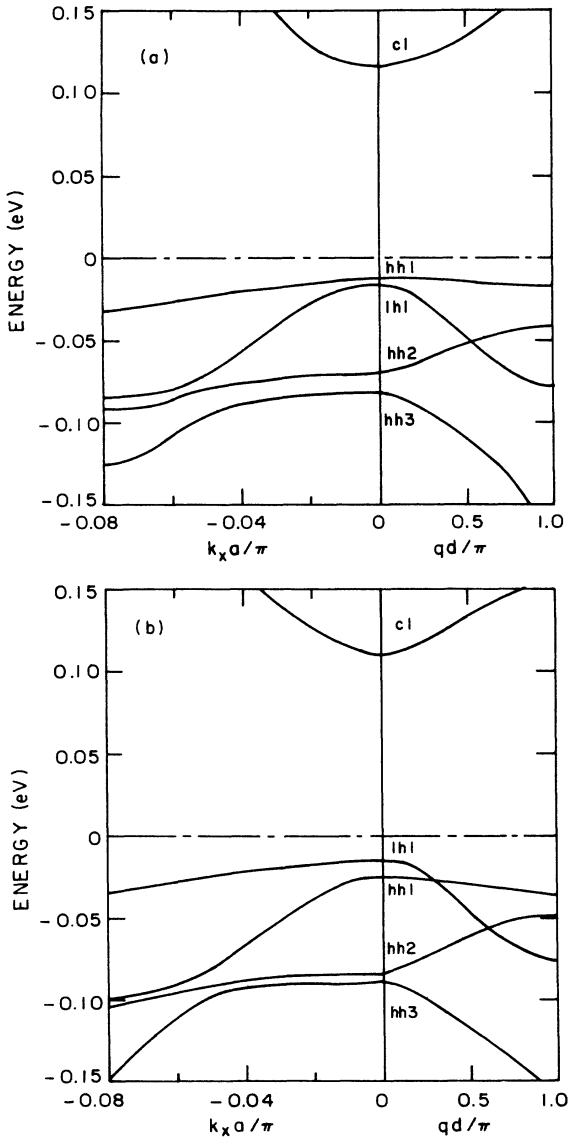

FIG. 3. The band structure of a HgTe/CdTe superlattice with growth axis along [001] and layer thicknesses (50 Å)/(40 Å). Band dispersion in the [001] (q) and [100] (k_x) directions is displayed (a) without strain, and (b) with strain.

meV compared to that in Ref. 8. If we were to use $a=-3.8$ eV, as in Wu and McGill,[39] the above-mentioned 8-meV disparity is found to disappear, and the overall pattern of the band structure is in excellent agreement with the tight-binding calculation of Ref. 8. Clearly, the ambiguity regarding the sign of a for HgTe has yet to be resolved.

IV. CONCLUSIONS

We have demonstrated the use of our new transfer-matrix method for the calculation of the band structure of superlattices in the framework of the EFA. We have shown that the results are in excellent agreement with those from the variational procedure employed by Altarelli[14] for GaAs/$Ga_{1-x}Al_xAs$ and with the tight-binding calculations of Schulman and Chang[8] for HgTe/CdTe.

Since the transfer-matrix method is based on the EFA, it has the corresponding advantage that the input parameters are those directly determined by experimentally measured optical and magnetooptical spectra of bulk materials. The effect of additional perturbations, such as an externally applied magnetic field or the built-in strain in superlattices, are easily incorporated into the $\mathbf{k}\cdot\mathbf{p}$ Hamiltonian and this involves no additional analysis in the transfer-matrix method. Furthermore, we are concerned with matrix analysis of matrices with much smaller dimensionality in the transfer-matrix scheme.

Applications of the method to superlattices grown in the [111] direction requires the rotation of the original Hamiltonian from the crystal axes to the "superlattice axes." After such a rotation is performed we can once again separate the new second-order differential equation into terms with corresponding coefficients for the derivative and the constant terms.

The transfer-matrix method provides a simple procedure to obtain the wave functions as a function of the coordinates. The wave functions are particularly useful in evaluating transition probabilities in magnetooptical spectra. Our preliminary analysis of our experimental spectra shows that half of the transitions allowed by the usual $\Delta n=\pm 1$ selection rule are essentially forbidden because their transition probabilities are negligible. Further analysis along these lines is in progress.

ACKNOWLEDGMENTS

This work was supported by the Strategic Defense Initiative of the Innovative Science and Technology Office (SDI-ISTO) [U.S. Naval Research Laboratory (NRL), Agent] under Grants No. N00014-87-K-2031 (L.R.R.) and No. N00014-86-C-2305 (K.H.Y. and R.L.A.).

APPENDIX

The complete 8×8 $\mathbf{k}\cdot\mathbf{p}$ Hamiltonian matrix is shown in Table III. We follow the notation and phase conventions used by Weiler.[21]

TABLE III. The 8×8 Kane Hamiltonian in the notation of Weiler (Ref. 21). The upper triangle of matrix elements is given, the lower triangle matrix elements being obtained by a complex conjugation of these matrix elements.

$$H_{11}=E_g+(F+\tfrac{1}{2})\mathbf{k}^2+\tfrac{1}{2}H_z$$
$$H_{12}=\frac{1}{\sqrt{2}}Pk^+$$
$$H_{13}=-\frac{1}{\sqrt{6}}Pk^-$$
$$H_{14}=\frac{1}{\sqrt{3}}Pk^-$$
$$H_{15}=\tfrac{1}{2}H^-$$
$$H_{16}=-(\tfrac{2}{3})^{1/2}Pk_z$$
$$H_{17}=0$$
$$H_{18}=\frac{1}{\sqrt{3}}Pk_z$$
$$H_{22}=-\tfrac{1}{2}\gamma_1\mathbf{k}^2+\tfrac{1}{2}\gamma_2F_3^1-\tfrac{3}{2}\kappa H_z$$
$$H_{23}=\tfrac{1}{2}\gamma_2F_3^2-i\frac{\sqrt{3}}{2}\gamma_3F_4^z$$
$$H_{24}=-\frac{1}{\sqrt{2}}\gamma_2F_3^2+i(\tfrac{3}{2})^{1/2}\gamma_3F_4^z$$
$$H_{25}=0$$
$$H_{26}=\frac{\sqrt{3}}{2}\gamma_3F_4^--\frac{\sqrt{3}}{2}\kappa H^-$$
$$H_{27}=0$$
$$H_{28}=-(\tfrac{3}{8})^{1/2}\gamma_3F_4^-+(\tfrac{3}{8})^{1/2}(\kappa+1)H^-$$
$$H_{33}=-\tfrac{1}{2}\gamma_1\mathbf{k}^2-\tfrac{1}{2}\gamma_2F_3^1+\tfrac{1}{2}\kappa H_z$$
$$H_{34}=-\frac{1}{\sqrt{2}}\gamma_2F_3^1-\frac{1}{\sqrt{2}}(\kappa+1)H_z$$
$$H_{35}=-(\tfrac{2}{3})^{1/2}Pk_z$$
$$H_{36}=-\kappa H^+$$
$$H_{37}=-\frac{\sqrt{3}}{2}\gamma_3F_4^--\frac{\sqrt{3}}{2}\kappa H^-$$
$$H_{38}=\frac{3}{\sqrt{8}}\gamma_3F_4^+-\frac{1}{\sqrt{8}}(\kappa+1)H^+$$
$$H_{44}=-\Delta-\tfrac{1}{2}\gamma_1\mathbf{k}^2+(\kappa+\tfrac{1}{2})H_z$$
$$H_{45}=-\frac{1}{\sqrt{3}}Pk_z$$
$$H_{46}=\frac{3}{\sqrt{8}}\gamma_3F_4^++\frac{1}{\sqrt{8}}(\kappa+1)H^+$$
$$H_{47}=-(\tfrac{3}{8})^{1/2}\gamma_3F_4^--(\tfrac{3}{8})^{1/2}(\kappa+1)H^-$$
$$H_{48}=-(\kappa+\tfrac{1}{2})H^+$$
$$H_{55}=E_g+(F+\tfrac{1}{2})\mathbf{k}^2-\tfrac{1}{2}H_z$$
$$H_{56}=\frac{1}{\sqrt{6}}Pk^+$$
$$H_{57}=-\frac{1}{\sqrt{2}}Pk^-$$
$$H_{58}=\frac{1}{\sqrt{3}}Pk^+$$
$$H_{66}=-\tfrac{1}{2}\gamma_1\mathbf{k}^2-\tfrac{1}{2}\gamma_2F_3^1-\tfrac{1}{2}\kappa H_z$$
$$H_{67}=\tfrac{1}{2}\gamma_2F_3^2-i\frac{\sqrt{3}}{2}\gamma_3F_4^z$$
$$H_{68}=\frac{1}{\sqrt{2}}\gamma_2F_3^1-\frac{1}{\sqrt{2}}(\kappa+1)H_z$$
$$H_{77}=-\tfrac{1}{2}\gamma_1\mathbf{k}^2+\tfrac{1}{2}\gamma_2F_3^1+\tfrac{3}{2}\kappa H_z$$
$$H_{78}=\frac{1}{\sqrt{2}}\gamma_2F_3^2+i(\tfrac{3}{2})^{1/2}\gamma_3F_4^z$$
$$H_{88}=-\Delta-\tfrac{1}{2}\gamma_1\mathbf{k}^2-(\kappa+\tfrac{1}{2})H_z$$

The cell-periodic wave functions $|j\rangle = u_{j,\mathbf{k}=0}$ are defined, in terms of the Kane basis functions, to be

$$
\begin{aligned}
&|1\rangle = |S\uparrow\rangle \ , \\
&|2\rangle = -(i/\sqrt{2})\,|(X+iY)\uparrow\rangle \ , \\
&|3\rangle = (i/\sqrt{6})\,|[(X-iY)\uparrow + 2Z\downarrow]\rangle \ , \\
&|4\rangle = -(i/\sqrt{3})\,|[(X-iY)\uparrow - Z\downarrow]\rangle \ , \\
&|5\rangle = |S\downarrow\rangle \ , \\
&|6\rangle = -(i/\sqrt{6})\,|[(X+iY)\downarrow - 2Z\uparrow]\rangle \ , \\
&|7\rangle = (i/\sqrt{2})\,|(X-iY)\downarrow\rangle \ , \\
&|8\rangle = -(i/\sqrt{3})\,|[(X+iY)\downarrow + Z\uparrow]\rangle \ .
\end{aligned}
\tag{A1}
$$

The parameters appearing in Table III are the band-edge energies E_g and Δ, relative to the Γ_8 valence band. The explicit inclusion of the interaction between the valence and conduction bands in the $\mathbf{k}\cdot\mathbf{p}$ approximation leads to modified Luttinger parameters discussed by Pidgeon and Brown.[20] The modified Luttinger parameters are given in terms of the usual Luttinger parameters γ_i^L, and κ^L by

$$
\begin{aligned}
\gamma_1 &= \gamma_1^L - \frac{E_P}{3E_g} \ , \\
\gamma_2 &= \gamma_2^L - \frac{E_P}{6E_g} \ , \\
\gamma_3 &= \gamma_3^L - \frac{E_P}{6E_g} \ ,
\end{aligned}
\tag{A2}
$$

and

$$
\kappa = \kappa^L - \frac{E_p}{6E_g} \ , \tag{A3}
$$

where

$$
E_P = 2m_0 p^2/\hbar^2 \ . \tag{A4}
$$

The parameter F appearing in the conduction-band kinetic energy term represents the contribution of higher conduction bands to the effective mass of the γ_6 conduction-band electron. In Table III we have set $\hbar = 1$, $c = 1$, $e = 1$, and $m_0 = 1$. Further abbreviations appearing in Table III are

$$
\begin{aligned}
\mathbf{k}^2 &= k_x^2 + k_y^2 + k_z^2 \ , \\
k^{\pm} &= k_x \pm i k_y \ , \\
F_3^1 &= 2k_z^2 - k_x^2 - k_y^2 \ , \\
F_3^2 &= \sqrt{3}(k_x^2 - k_y^2) \ , \\
F_4^{\pm} &= k_z k^{\pm} + k^{\pm} k_z \ , \\
F_4^z &= k_x k_y + k_y k_x \ , \\
H_z &= i(k_x k_y - k_y k_x) \ , \\
H^{\pm} &= \pm(k^{\pm} k_z - k_z k^{\pm}) \ .
\end{aligned}
\tag{A5}
$$

In the absence of a magnetic field the H terms given above and the terms with the parameter κ will be zero.

*Also at Lincoln Laboratory, Massachusetts Institute of Technology, Lexington, MA 02173.

[1] J. N. Schulman and T. C. McGill, Phys. Rev. Lett **39**, 1680 (1977); Phys. Rev. B **19**, 6341 (1979).

[2] G. A. Sai-Halasz, L. Esaki, and W. A. Harrison, Phys. Rev. B **18**, 2812 (1978).

[3] I. Ivanov and J. Pollmann, Solid State Commun. **32**, 869 (1979).

[4] A. Madhukar and R. N. Nucho, Solid State Commun. **32**, 331 (1979); A. Madhukar and J. Delgado, *ibid.* **37**, 199 (1981).

[5] G. C. Osbourn, J. Appl. Phys. **53**, 1586 (1982).

[6] J. N. Schulman and Y.-C. Chang, Phys. Rev. B **24**, 4445 (1981).

[7] J. N. Schulman and Y.-C. Chang, Phys. Rev. B **31**, 2056 (1985); Y.-C. Chang and J. N. Schulman, *ibid.* **31**, 2069 (1985).

[8] J. N. Schulman and Y.-C. Chang, Phys. Rev. B **33**, 2594 (1986).

[9] G. Bastard, Phys. Rev. B **24**, 5693 (1981).

[10] G. Bastard, Phys. Rev. B **25**, 7584 (1982).

[11] S. R. White and L. J. Sham, Phys. Rev. Lett. **47**, 879 (1981).

[12] M. Altarelli, Phys. Rev. B **28**, 842 (1983).

[13] M. Altarelli, U. Ekenberg, and A. Fasolino, Phys. Rev. B **32**, 5138 (1985).

[14] M. Altarelli, J. Lumin. **30**, 472 (1985).

[15] J. M. Berroir, Y. Guldner, J. P. Vieren, M. Voos, and J. P. Faurie, Phys. Rev. B **34**, 891 (1986).

[16] E. O. Kane, in *Semiconductors and Semimetals,* edited by R. K. Willardson and A. C. Beer (Academic, New York, 1966), Vol. 1, p. 75.

[17] R. de L. Kronig and W. G. Penney, Proc. R. Soc. London, Ser. A **130**, 499 (1931).

[18] J. M. Luttinger and W. Kohn, Phys. Rev. **97**, 869 (1955).

[19] J. M. Luttinger, Phys. Rev. **102**, 1030 (1956).

[20] C. R. Pidgeon and R. N. Brown, Phys. Rev. **146**, 575 (1966).

[21] M. H. Weiler, in *Semiconductors and Semimetals,* edited by R. K. Willardson and A. C. Beer (Academic, New York, 1981), Vol. 16, p. 119.

[22] B. T. Smith, *et al.*, *Matrix Eigensystem Routines*—EISPACK *Guide,* 2nd ed., Vol. 6 of *Lecture Notes in Computer Science* (Springer-Verlag, New York, 1976).

[23] J. T. Dongarra *et al.*, LINPACK *Users Guide* (Society for Industrial and Applied Mathematics, Philadelphia, 1979).

[24] C. Moler and C. van Loan, SIAM Rev. **20**, 801 (1978).

[25] A. Onton, in *Festkörperprobleme XIII, Advances in Solid State Physics,* edited by H. S. Queisser (Vieweg, Braunschweig, 1973), p. 59.

[26] *Landolt-Börnstein Numerical Data and Functional Relationships in Science and Technology,* Group III, Vol. 17 edited by O. Madelung (Springer, Berlin, 1982).

[27] R. C. Miller, D. A. Kleinman, and A. C. Gossard, Phys. Rev. B **29**, 7085 (1984).

[28]R. Dingle, A. C. Gossard, and W. Wiegmann, Phys. Rev. Lett. **34**, 1327 (1975).
[29]L. M. Roth, B. Lax, and S. Zwerdling, Phys. Rev. **114**, 90 (1959).
[30]R. L. Aggarwal, in *Semiconductors and Semimetals,* edited by R. K. Willardson and A. C. Beer (Academic, New York, 1972), Vol. 9, p. 151.
[31]S. P. Kowalczyk, J. T. Cheung, E. A. Kraut, and R. W. Grant, Phys. Rev. Lett. **56**, 1605 (1986); T. M. Duc, C. Hsu, and J. P. Faurie, *ibid.* **58**, 1127 (1987); also see, J. Meyer *et al.*, Phys. Rev. B **38**, 2204 (1988).
[32]S. H. Wei and A. Zunger, Phys. Rev. Lett. **59**, 144 (1987).
[33]R. Yoshizaki and S. Tanaka, Solid State Commun. **20**, 909 (1979).
[34]K. Takita and G. Landwehr, Phys. Status Solidi B **106**, 259 (1981).
[35]G. L. Bir and G. E. Pikus, *Symmetry and Strain-Induced Effects in Semiconductors* (Wiley, New York, 1974).
[36]G. Y. Wu (private communication).
[37]T. Alper and G. A. Saunders, J. Phys. Chem. **28**, 1637 (1967).
[38]G. Weill and C. Verie, C. R. Acad. Sci. (France) **263**, 463 (1966).
[39]G. Y. Wu and T. C. McGill, Appl. Phys. Lett. **47**, 634 (1985).